Effects of the Cosurfactant 1-Butanol and Feed Composition on Nanoparticle Properties Produced by Microemulsion Copolymerization of Styrene and Methyl Methacrylate

Daniel P. Otto,[1,2] Hermanus C. M. Vosloo,[2] Wilna Liebenberg,[3] Melgardt M. de Villiers[1]

[1]*School of Pharmacy, Pharmaceutical Sciences Division, University of Wisconsin - Madison, Wisconsin 53705*
[2]*SST Catalysis and Synthesis Research Group, School of Chemistry, North-West University, Potchefstroom 2520, South Africa*
[3]*Unit for Drug Research and Development, Faculty of Health Sciences, North-West University, Potchefstroom 2520, South Africa*

Received 1 June 2007; accepted 5 October 2007
DOI 10.1002/app.27536
Published online 10 December 2007 in Wiley InterScience (www.interscience.wiley.com).

ABSTRACT: The concentration of the cosurfactant 1-butanol (BuOH) determined the polymer weight and size for a series of poly(styrene-*co*-methyl methacrylate)s (P(St-*co*-MMA)) synthesized by the free-radical (o/w) microemulsion technique. A factorial design established the levels of the experimental conditions for the polymerization i.e., concentration of the surfactant, sodium dodecyl sulfate (SDS); concentration of the cosurfactant, BuOH; temperature and ratio of the styrene (St) to methyl methacrylate (MMA). An increase in the weight-average molecular weight (M_w) and number-average molecular weight (M_n) was observed in the P(St-*co*-MMA) series with an increase in BuOH concentration from 1 to 5 wt %. These effects could arise from the micellar aggregation induced by interfacial BuOH. The unique micellar conditions could be exploited to synthesize copolymers of varying molecular weight and size. Additionally, the composition of the copolymers was virtually templates of the feed composition. © 2007 Wiley Periodicals, Inc. J Appl Polym Sci 107: 3950–3962, 2008

Key words: microemulsion copolymerization; cosurfactant; GPC-MALLS; ATR-FTIR

INTRODUCTION

Microemulsions have been studied extensively over the years and provided a unique polymerization technique in the 1980s for the production of homopolymers.[1,2] Subsequently, the method was applied to fabricate copolymers in the following decade and since then various reports have been published that illustrated the synthesis of high molecular weight polymers showing high monomer conversion levels.[3–6] Since microemulsions are thermodynamically stable and require virtually no agitation to disperse the oil, water, and surfactant pseudophases, it provides an important advantage over the traditional or coarse emulsions that are only kinematically stable upon significant agitation.[7]

The addition of short-chain alcohols such as 1-butanol (BuOH), 1-pentanol, and 1-hexanol provides additional stability of the microemulsions and these are often added as cosurfactants into polymerization mixtures. These cosurfactants act on the micellar surface where they can displace surfactant molecules from the micellar surface, resulting in a decrease in the CMC.[8–10] Factors that influence the effect and localization of alcohol cosurfactants are alcohol chain length,[11,12] chain branching, number of functional hydroxyl groups,[13–15] and aromaticity.[16] For example, hydrophilic alcohols partitioned to the bulk dispersion phase whereas long-chain, lipophilic alcohols partitioned to the lipophilic micellar core resulting in larger micellar cores. Therefore, the ideal alcohol cosurfactant would reside in the interface with no significant partitioning to the continuous or dispersed pseudophases.

Since *n*-butanol, pentanol, and even hexanol reside at the interface, they would be the cosurfactants of choice.[6,17–19,20,21] However, the inclusion of these short chain alcohols as cosurfactants into microemulsion copolymerization systems can result in seemingly inexplicable changes in molecular weight as a consequence of the variation of the cosurfactant concentration. Although not clearly understood, some explanations for these observations included the macroradical chain transfer to the cosurfactant and film formation around the surface of the micelle that shield polymer radicals.[22–24]

In this study, a series of poly(styrene-*co*-methyl methacrylate) (P(St-*co*-MMA)) was synthesized under various concentrations of *n*-butanol, surfactant, temperature, and monomer mixture composi-

Correspondence to: D. P. Otto (dotto@wisc.edu).

tion. The aim was to investigate the effects of the experimental factors on the molecular weight, copolymer particle size, and chemical composition of the copolymer. The cosurfactant concentration prevailed as the primary determinant of molecular weight and size, while the monomer feed ratio significantly affected chemical composition of the copolymers.

EXPERIMENTAL

Materials

Methyl methacrylate (MMA) was donated by Degussa (Düsseldorf, Germany) and styrene (St) was purchased from Merck (Modderfontein, South Africa). The MMA and St were purified prior to polymerization by adsorption of the inhibitors onto dried neutral alumina-packed glass columns. A slightly yellow band was noted for styrene at the top of the alumina column. 1-Butanol (BuOH, >99%) was purchased from Merck and incorporated as cosurfactant. Ultra pure sodium dodecyl sulfate (SDS, >99%) and hydroquinone (HQ) were obtained from Sigma-Aldrich (Kempton Park, South Africa). Potassium persulfate (KPS) was purchased from Sigma-Aldrich and employed as reaction initiator and double-deionized water was utilized to produce the dispersion medium.

Synthesis procedure and latex treatment

A report by Tauer et al.[25] was used as a guide to determine the compositions of the microemulsion by variation of the concentration of monomer, surfactant, and dispersion media. A 500-mL three-necked flask was charged with the requisite quantities of the reagents according to a fractional 3-level-4-factor factorial design, to comprise a final mixture weight of 100 g (Table I). Water (100 g), 500 mg KPS (all experiments), SDS, and BuOH were added to a three-necked flask equipped with a condenser and thermometer and was maintained at the desired reaction temperature (60°C, 70°C, or 80 °C ± 1°C) to decompose KPS to produce initiator radicals. The dissociation of the initiator KPS necessitated a temperature of at least 60°C and this was therefore selected as the minimum reaction temperature. The reaction proceeds with KPS providing the initiator radicals to form primary monomer radicals that propagate the polymer chains. The mixture was magnetically stirred at 500 rpm while continuously purged with filtered nitrogen. After 15 min of nitrogen purging at the specified reaction temperature, 6 g of degassed, vortex-mixed monomer reagents (in the desired ratio) were added to the dispersion medium through a syringe fitted with a 0.22 μm Cameo™ Teflon® filter (Sigma-Aldrich). After monomer addition, colloidal particle growth was observed from the slightly blue, translucent microemulsions. Figure 1 renders a graphical depiction of the reaction environment in the three-neck flask. A reaction time of 120 min was employed for all experiments and after this period, the reaction was quenched with an excess of HQ. The design and procedures were performed in duplicate to render 54 (2 sets of 27) experiments.

TABLE I
The Factorial Design That was Employed to Determine Mixture Composition and Reaction Conditions

	Concentration (wt %)		
Factor	Low	Intermediate	High
SDS	2	4	8
BuOH	1	3	5
St[a] (%)	60	70	80
Temperature (°C)	60	70	80

Experiments were conducted for one level for each factor.

[a] %St in monomer mixture with a total weight of 6 g monomer mixture. This ratio was converted to percent mole fraction of St (f_{St}) in the text and graphs.

The polymer latex was collected in 50 cm^3 centrifuge tubes in an excess of methanol and allowed to cool to room temperature. The fractions were then centrifuged at 3500 rpm for 10 min, redispersed, and washed in fresh aliquots of methanol. The centrifugation and washing cycle was repeated until the latex could no longer be redispersed. Subsequently, the latex was dried in a fume hood and then pulverized to a fine, white powder. Furthermore, these powders were dried under a vacuum of 13 mbar for 24 h at a regulated temperature of 40°C (well below T_g of the copolymers ~ 90–100°C). Finally, the dried polymer samples were stored in opaque, air tight containers.

GPC-MALLS

A DAWN® DSP photometer (Wyatt Corp., Santa Barbara, CA) was employed for absolute weight measurements utilizing a size exclusion chromatography setup. The multi-angle laser light scattering (MALLS) detector consisted of a 5 mW He-Ne laser that illuminated samples at a wave-length of 632.8 nm. The MALLS detector was carefully calibrated with filtered HPLC grade toluene (BDH, Merck) and then normalized with an isotropic scattering poly (styrene) (PS) standard (M_w 30,000 g mol^{-1}, polydispersity < 1.05, Pressure Chemical Company, Pittsburgh, PA, USA). The MALLS was connected to a refractive index (RI) detector (Agilent® 1100 series) to determine concentration of the eluting species. On-line determination of the specific refractive index (dn/dc) was performed as reported elsewhere[26–28] by

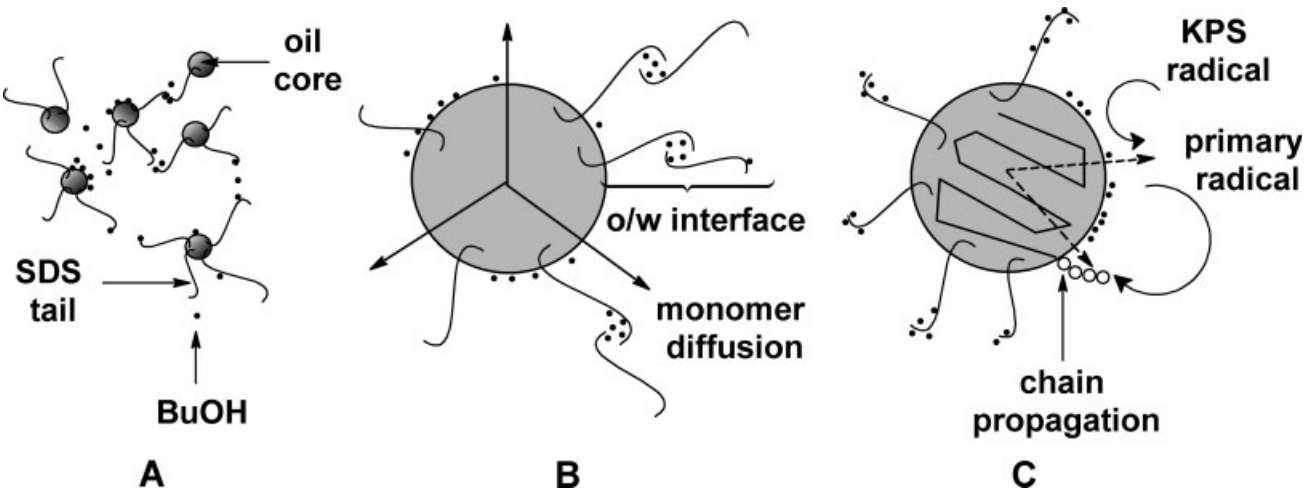

Figure 1 Representation of the micellar reaction environment in the three-neck flask. (A) Micelles are formed and BuOH displaces SDS from surface or results in micellar aggregation. (B) Monomer diffuses from the micelle core to the (o/w) interface. (C) Initiator radicals engage monomer molecules in the interface to form primary radicals that initiate chain propagation in the micelle by recruitment of additional monomer molecules (Components are not drawn to scale).

addition of a small, accurately known quantity of a low weight polystyrene standard (M_w 2550 g mol^{-1}, $M_w/M_n < 1.05$, Pressure Chemical) to the polymer sample.

Samples were prepared at a concentration of 3 mg mL^{-1} by sonication of the appropriate quantities of polymer and *dn/dc* standard in HPLC-grade THF for 10 min. Sample solutions were filtered utilizing Millipore® 0.45 μm (Microsep (Pty), Sandton, South Africa) filters that were chemically resistant to THF. All samples were prepared and injected in duplicate.

An HPLC (Agilent® 1100) injected 100 μL polymer samples (3 mg/mL) prepared in THF into the GPC columns coupled in series. The columns (purchased from Separations Scientific CC, Honeydew, South Africa) comprised of a PLGel® mixed bed type C™ (7.6 mm × 300 mm, exclusion range 300–2,000,000 g mol^{-1}, particle size of 5 μm) and a Phenogel™ (Phenomenex®, 7.8 mm × 300 mm, exclusion range > 5000 g mol^{-1}, particle size of 5 μm). HPLC grade THF (BDH) was employed as elution liquid at a regulated flow rate of 1 mL min^{-1} while maintaining the system temperature at 30°C.

ASTRA™ for Windows® version 4.73.04 (Wyatt Corp.) was utilized to record, overlay, and analyze the MALLS and RI detector signals. The software calculated the number-average molecular weight (M_n), the weight-average molecular weight (M_w), the radius of gyration ($\langle s^2 \rangle^{1/2}$), and the conformation of the copolymer in the theta solvent, tetrahydrofuran. The computations were made according to the Zimm formalism employing all scattering angles from 17 to 155°.

The molecular weight of each slice was calculated according to the Zimm-Stockmayer equation[29–31] from which the averages M_n and M_w were ultimately derived eq. (1):

$$\frac{R_\Theta}{Kc} = \mathrm{MP}(\Theta) - 2A_2cM^2P^2(\Theta) + \cdots \quad (1)$$

where M is the molecular weight of a slice of the sample chromatogram, R_Θ is the excess Rayleigh ratio at the scattering angle Θ. Additionally, the wavelength and scattering angle-dependent particle scattering factor is represented by $P(\Theta)$. Furthermore, the concentration of the particles is denoted as c (determined with the refractive index detector) and A_2 is the second virial coefficient (osmotic pressure to light scattering), which becomes negligible at low concentrations as employed here). The constant K was derived by the software from eq. (2):

$$K = \frac{4\pi^2 n_0^2}{\lambda_0^4 N_A}\left(\frac{dn}{dc}\right)^2 \quad (2)$$

where the refractive index of the solvent in vacuum is n_0 at the incident wavelength of the vertically polarized laser radiation, λ_0, the Avogadro number is N_A, and the specific refractive increment of the polymer is dn/dc.

Conformational analysis was performed by evaluation of the linear segment of the data if plotted as a double-logarithmic plot and fitted to a power law regression according to eq. (3):[32,33]

$$\langle s^2 \rangle^{1/2} \propto M_w^q \quad (3)$$

where the z-average root mean square $\langle s^2 \rangle^{1/2}$ radius to was related weight-average molecular weight M_w.

The exponent q is derived from the slope by fitting a power law regression on the linear segment of the double-logarithmic plot, revealing the chain conformation of the polymers. For the theoretical condition of $q = 1/3$ a spherical, compact conformation of the chain is demonstrated. Under ideal condition where $q = 1/2$ theta conditions prevail indicating that a cluster of chains has been separated by solvent; however, limited chain expansion is evidenced and a more compact conformation is still present. A chain that revealed $0.5 < q \leq 0.6$ indicates that a random coil conformation is assumed and the solvent resulted in some degree of swelling of the species. Values of $q > 3/5$ indicate that the chain assumed a rigid, rod-like conformation possibly with a constant diameter.

Calculation of reliable conformation exponents necessitated eliminating size values and their corresponding weights with a correction factor according to eq. (4):

$$\langle s^2 \rangle_{\text{lim}}^{1/2} = \frac{I_s}{20n} \tag{4}$$

where I_s is representative of the source wavelength. The limit at which a reliable radius of gyration could be determined *in vacuo* is set at 1/20th of the I_s. Below this limit, intensity of Rayleigh scattering declines as Debye scattering prevails at this limit.[34,35] Additionally, scattering becomes isotropic below 10 nm and therefore, angle-independent. However, in reality the refractive index of the solvent, n, lowers the limit. The limit for reliable $\langle s^2 \rangle^{1/2}$ in these calculations was therefore determined at $\sim$ 20 nm. In addition, adjustment of the start and endpoints of the light scattering peak made data evaluation possible in the section of low dispersity as well as excluded the minimum radius limit and uncertainties at the high end of the log-log plot of $\langle s^2 \rangle^{1/2}$ versus M_w.

ATR-FTIR

Attenuated total reflectance Fourier transform infrared spectroscopy (ATR-FTIR) is a popular method for quantitative analysis of copolymer composition.[36–39] The (ATR) procedures were performed in the mid-IR region and spectra were recorded in the region 4000–650 cm^{-1}. A Bruker Equinox™ 55 (Bruker, Ettlingen, Germany) IR spectrometer was employed for all data collections. The spectrometer utilized a He-Ne laser operated at 632.8 nm and was equipped with a micro ATR sampling accessory containing a ZnSe crystal. Spectra were recorded by coaddition of 32 scans with a spectral resolution of 4 cm^{-1}. Bruker Opus™ 5.1 software was employed to collect and process the ATR spectra. Baseline correction was performed on all spectra. The spectrometer was operated under continuous N_2 purge.

Low weight homopolymers of low polydispersity were selected to prepare homopolymer blends varying in composition. Suitable quantities of poly (methyl methacrylate) PMMA and PS were dissolved in THF and then precipitated. The polymer blends were vacuum-dried for at least 12 h. Subsequently, the precipitates were ground to produce fine powders. These standards were analyzed directly on the ATR crystal and four spectra were collected per standard. Calibration curves were constructed by plotting the absorbance ratio of two peaks, which could be assigned unambiguously to either the styrene monomer ($\sim$ 699 cm^{-1} for the out of plane bending of the phenyl ring) and for the methacrylate monomer (saturated alkyl ester carbonyl stretch at $\sim$ 1729 cm^{-1}), versus the mole fraction ratio (f_{St}) of the two homopolymers employed in each set.

Subsequently, four spectra of the experimental samples were acquired by recording two spectra of a copolymer sample followed by analysis of a duplicate sample of the same specimen.

Calculations and statistics

STATISTICA 7.1 (Statsoft, Tulsa, OK) was used to evaluate data for possible linear (denoted by 'L') or nonlinear (denoted by 'Q') single factor effects as well as for two-way linear by linear interactions between the experimental factors and to determine the significance of factor influences by Pareto density analysis.

The Pareto principle states that in a population of factors that contribute to a common effect, only a few of these factors would contribute significantly to the observed effect.[40] In this study the population of factors were SDS, BuOH, temperature, and monomer feed ratio; the two-way linear interactions between these variables and the characteristics of the single factor contributions i.e., linear or quadratic. The analytical results obtained through GPC-MALLS and ATR-FTIR were substituted into the factorial design and analyzed by the statistical software. The Pareto analysis was performed to determine which factor(s) dominated the measured response i.e., M_n. On the basis of this analysis, explanations for the observations were sought and illustrated through surface plots.

The standard Pareto density function is described by eq. (5):

$$f(x) = \frac{c}{x^{c+1}}, \quad 1 \leq x, \; c > 1 \tag{5}$$

where the shape parameter of the population density distribution (spread of contributions of experimental

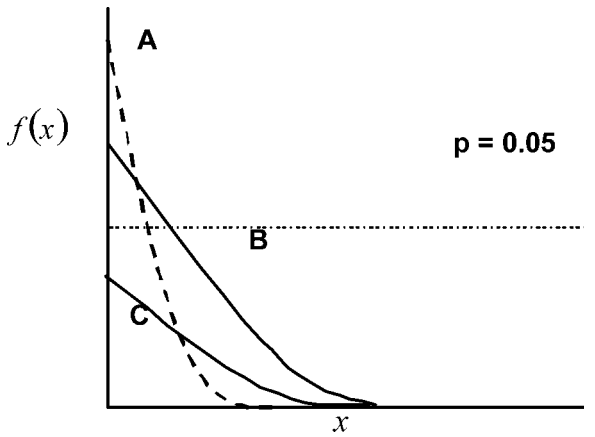

Figure 2 Pareto graphs of (A) Low c, narrow density of distribution with a few factors exceeding $p = 0.05$; high Pareto coefficients. (B) Intermediate c, low density with a number of factors proving significant; intermediate Pareto coefficients. The higher c becomes, the broader the density distribution and the less significant the factors, x become until none prove significant as in curve C [eq. (5)].

factors to the effect) is c and the factor(s) that contributed to the measurement density is x. The value of $f(x)$ should exceed a specified value at a specified confidence interval should the factor prove significant. In this study we used the absolute values of the Pareto coefficients and these should exceed 2.023 as the minimum for significance at the 95% confidence interval. Figure 2 renders the influence of three different shape factors and a hypothetical density of $f(x)$.

RESULTS AND DISCUSSION

Synthesis, characterization, and processing of raw data

All the reactions produced polymeric materials under the conditions shown in Table I. Subsequently, 54 products were produced and their molecular weights and radii of gyration were characterized with GPC-MALLS. Compositional content of St and MMA was determined by ATR-FTIR analysis. Duplicate samples were analyzed on different days (due to the extensive analysis period required) and these results did not vary significantly, indicating that polymers remained stable.

Figure 3 illustrates an example of the weight distributions as a function of elution volume. The weight distribution was obtained by converting each data point of the chromatogram and corresponding light scattering data to M_w [eq. (1)] and plotting log M_w versus elution volume. Note that the elution volume agreed with the chromatograms and that no secondary peaks or weight distributions were observed for the dn/dc standard. As an example of the results an excerpt of the results obtained by GPC-MALLS is listed in Table II and shows only results of experiments performed with 2% SDS (data for 4 and 8% SDS classifications or for any other factor classifications are not shown; however, were automatically compiled and considered by the statistical software). These results (Table II and the remainder of categorizations) were then substituted into the factorial design.

Although the Pareto method had its origins in economical science,[41] it has been applied in various recent polymer studies to determine the contribution of experimental factors to a common effect and to optimize experimental parameters for polymerization reactions.[42–44] As an example, the Pareto graph of standardized factor effects on M_n for P(St-*co*-MMA) is shown in Figure 4. Closer inspection of the Pareto analysis indicated that a positive, linear effect was observed for M_n measurements attributed to an increase in BuOH concentration as denoted by 'L' and a positive value of the Pareto coefficient of 5.256 (Fig. 4). In contrast, the effect of temperature proved to be significantly quadratic as denoted by 'Q' and a minimum turning point was revealed by the negative sign preceding the coefficient of 2.736 (Fig. 4).

Subsequently, the Pareto coefficients were obtained for all responses and tabulated (Table III). The Pareto coefficients calculated in this experimental design needed to exceed a minimum value of 2.023 to prove significant at a 95% confidence interval (Fig. 4 and Table III). Additionally, a positive or negative sign preceded the coefficient and indicated an increase or decrease in the measured responses

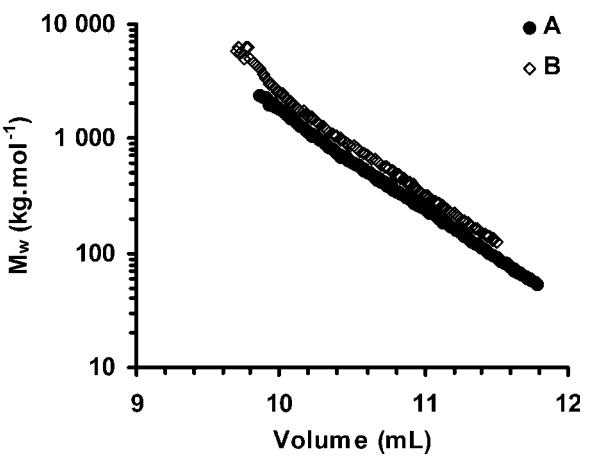

Figure 3 The M_w distribution of two synthesized polymer samples (A) 2% SDS, 1% BuOH, f_{St} of 69.2%, 80°C and (B) 8% SDS, 3% BuOH, f_{St} 69.2%, 80°C. The dn/dc standard could not be observed, confirming that it did not interfere with the sample analysis and weight distribution. Each point was calculated from light scattering data [eq. (1)] by ASTRA™.

TABLE II
Excerpt of the Results for P(St-*co*-MMA) as Categorized by 2% SDS[a]

Reaction conditions			Results						
BuOH (%)	°C	f_{St} (%)	St (%)	MMA (%)	M_n	M_w	M_w/M_n	$\langle s^2\rangle^{1/2}$ (nm)	q
1	60	59.0	56 ± 10	44 ± 10	214.9 ± 17	362.3 ± 29	1.74 ± 0.2	26.5 ± 0.2	0.449 ± 0.03
	70	79.4	57 ± 2.2	43 ± 2.2	164.1 ± 3.0	322.5 ± 27	1.98 ± 0.2	27.9 ± 2.2	0.484 ± 0.03
	80	69.2	61 ± 2.5	39 ± 2.5	160.3 ± 17	274.4 ± 49	1.79 ± 0.4	23.2 ± 0.4	0.460 ± 0.04
3	60	79.4	72 ± 7.6	28 ± 7.6	294.3 ± 10	493.4 ± 14	1.70 ± 0.1	35.7 ± 0.2	0.465 ± 0.01
	70	69.2	58 ± 5.2	42 ± 5.2	133.7 ± 13	236.9 ± 31	1.72 ± 0.3	21.6 ± 2.4	0.465 ± 0.01
	80	59.0	53 ± 1.4	47 ± 1.4	300.7 ± 38	499.6 ± 49	1.60 ± 0.3	32.9 ± 2.1	0.497 ± 0.01
5	60	69.2	65 ± 8.1	35 ± 8.1	343.0 ± 27	594.9 ± 42	1.79 ± 0.2	39.3 ± 1.6	0.504 ± 0.04
	70	59.0	49 ± 1.4	51 ± 1.4	262.8 ± 23	394.2 ± 7.0	1.50 ± 0.2	30.9 ± 1.9	0.503 ± 0.00
	80	79.4	73 ± 9.2	27 ± 9.2	452.4 ± 26	733.1 ± 30	1.66 ± 0.1	46.5 ± 3.3	0.463 ± 0.02

[a] All molecular weight values reported in kg mol^{-1}.

and in the case of nonlinearity a maximum or minimum turning point in the curvature.

The effect of BuOH (L) [Fig. 5(A)] and quadratic effect temperature (Q), [Fig. 5(B)] were constructed from the data in Table II. By addition (automatic function of the statistical software) of the remaining classifications i.e., 4 and 8% SDS (or any other set of classifications) to these graphs, surface plots resulted and several of these were discussed in the text here.

Compositional analysis

ATR-FTIR analysis revealed two spectral regions of interest for the analysis of the copolymers. The out-of-plane ring deformation of the phenyl ring in the Styrene (St) monomer was clearly observed at ~ 699 cm^{-1} and the stretching of the saturated ester carbonyl group of the methacrylate monomer at ~ 1729 cm^{-1} (Fig. 6). Several spectra were recorded and calibration curves constructed. The St/MMA standards showed strong linearity with $r^2 > 0.99$ for calibration curves with compositions in the range of the monomer content of the synthesized copolymers. On average, the copolymers contained ~ 8% less St than was included in the feed (Table I and Fig. 7). The mixtures containing 59% St in the feed produced copolymers containing 53% St as a series average. The 69% feed mixtures yielded copolymers containing 61% St and the maximum feed of 79% resulting in copolymers containing 71% (with the series showing $r^2 = 0.9944$). This slight compositional drift arose from the slightly higher reactivity ratio of the MMA compared with the St monomer,[45] favoring MMA incorporation marginally. Therefore, the feed served as an approximate template for the composition of the copolymer.

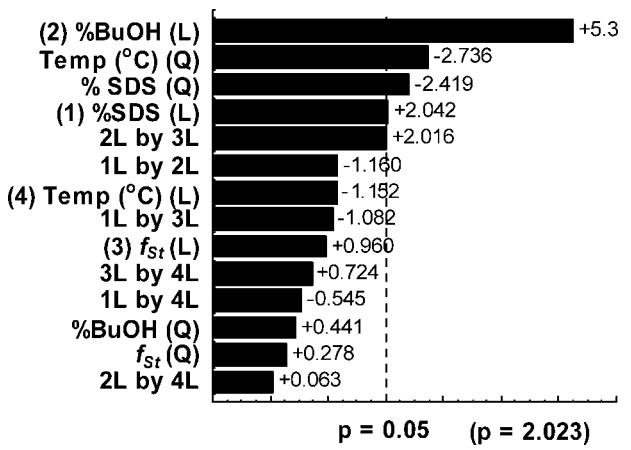

Figure 4 Pareto graph of standardized factor effects on M_n for P(St-*co*-MMA). Linear effects are denoted with the capital 'L' and the nonlinear (or quadratic) effects by capital 'Q'. Any interaction is indicated by the term, 'by'. The number that preceded a given factor was generated from the number of the column in which data was entered in the spreadsheet and should not be mistaken for the ranking of the effect.

Molecular weight of P(St-*co*-MMA)

M_n relates to the number of particles that were encountered in the eluted samples, therefore also indicates proportionality to the number of micellar reactors that were involved in particle evolution. It was apparent from Pareto analysis (Fig. 4, Table III) that the effect of BuOH dominated the measured response for M_n. A positive, linear effect was observed for BuOH [Fig. 8(A)] on M_n as was made apparent by the Pareto coefficient (L, +5.526) and significantly overshadowed the nonlinear effects of temperature (Q, −2.736) and SDS (Q, +2.419) (Table III). A linear increase in M_n (102.0–470.7 kg mol^{-1}, calculated as the averages of all 18 values obtained at a specified concentration of BuOH) was observed as a consequence of a linear increase in the cosurfactant concentration (1–5%). Temperature resulted in a nonlinear continuance with minimum turning points as seen from the negative sign before the coefficient [Fig. 8(A), Table III]. Additionally, the surfactant (SDS) had a predominantly nonlinear effect with a minimum turning point if compared with its linear

TABLE III
Pareto Coefficients for the Full Population of P(St-*co*-MMA) Samples

	P(St-*co*-MMA)					
Factor/interaction[a]	M_n	M_w	M_w/M_n	$\langle s^2\rangle^{1/2}$	q	St (%)
(1) SDS (L)	+2.042*	+2.096*	+2.326*	+0.784	−0.530	+0.535
SDS (Q)	−2.418*	−2.257*	+1.825	−0.457	−1.156	+1.077
(2) BuOH (L)	+5.256*	+5.086*	−2.892*	+5.249*	+1.317	+1.025
BuOH (Q)	+0.441	+0.082	−1.874	+0.340	+1.785	+0.043
(3) f_{St} (L)	+0.960	+0.743	−0.661	+0.660	−0.232	+9.088*
f_{St} (Q)	+0.278	+0.354	−0.465	−0.048	+0.531	−0.682
(4) Temperature (L)	−1.152	−1.281	+0.325	−1.631	−1.295	−0.336
Temperature (Q)	−2.736*	−2.369*	+2.182*	−3.005*	+0.840	−1.160
1L by 2L	−1.160	−1.020	+0.526	−0.794	−1.447	−1.346
1L by 3L	−1.081	−1.571	−1.873	−2.446*	+0.820	+1.062
1L by 4L	−0.545	−0.385	+0.437	−0.935	−0.942	+1.161
2L by 3L	+2.016	+1.731	−1.767	+1.027	−1.194	+1.987
2L by 4L	+0.063	+0.148	+0.133	+0.553	+0.381	+0.378
3L by 4L	+0.724	+0.433	−1.991	+0.643	−0.324	+0.556

For explanations of the abbreviations used see the experimental section.
* Effects are significant ($P < 0.05$) if the Pareto coefficient exceeds an absolute value of 2.023.
[a] Effects of the factors/interactions not noted according to rank.

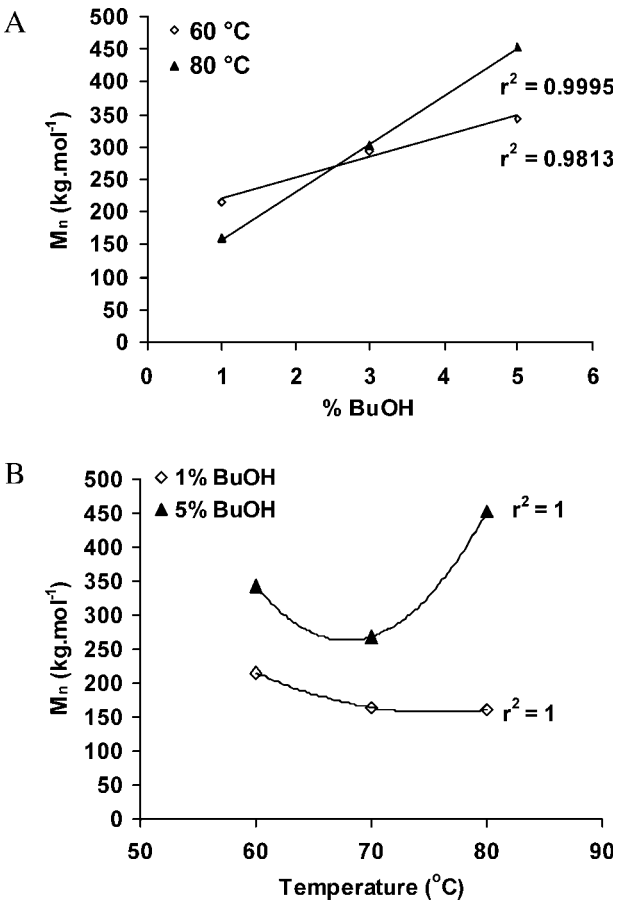

Figure 5 Illustration of (A) the linear effect of BuOH and (B) the quadratic effect of temperature (°C) on the response measured for M_n by fitting a second degree polynomial curve (linear fitting showed $r^2 \sim 0.80$ for 1% BuOH). For both A and B a sample of the data was taken and categorized by 2% sodium dodecyl sulfate (Table II) to construct the graphs.

effect (Fig. 4). Pareto coefficients of SDS (Q, −2.419 and L + 2.042) were of comparable magnitude and closely related in magnitude (Table III).

Clearly a larger number of particles was present at 1% BuOH (M_n of 102.0 kg mol^{-1} indicated a large number of particles) compared with 5% (M_n of 470 kg mol^{-1} demonstrated that the particle number was smaller).

Butanol is a cosurfactant that preferentially resides in the interface at the micellar surface therefore might affect the number of active micellar reactors.[46] The microemulsion essentially consists of three liquid pseudophases, i.e., oil, water, and a third pseudophase that is introduced by addition of the alcohol. This alcohol pseudophase could self-associate

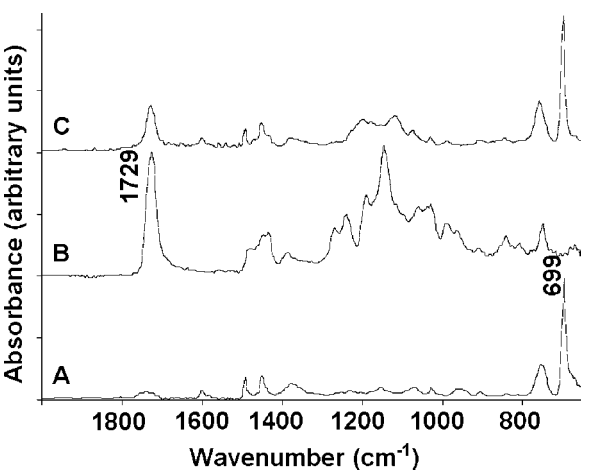

Figure 6 Expanded ATR-FTIR spectra of (A) PS (phenyl ring out of plane bending at 699 cm^{-1}), (B) PMMA (saturated ester carbonyl stretching at 1729 cm^{-1}), and (C) P(St-*co*-MMA) comprised of 56% styrene and 44% MMA.

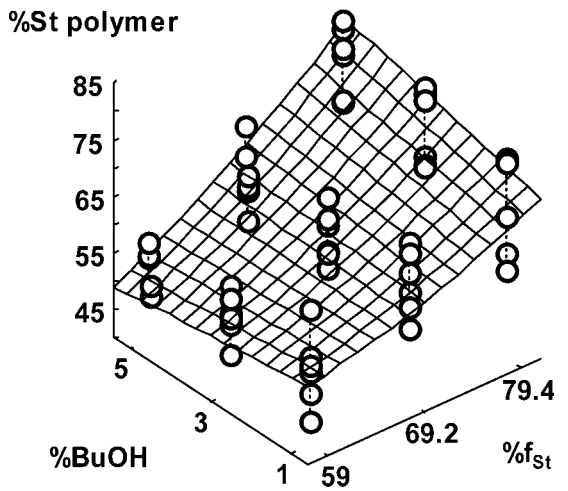

Figure 7 Effects of f_{St} and % BuOH on % St in P(St-*co*-MMA).

and since it is located preferentially in the interface, it would also associate the micelles into a denser structure. In fact based on its HLB value of 7.0, BuOH was shown to reside in the interface of Triton X-114 micelles.[47]

The linear increase in M_n suggested that a cluster of micelles formed with some of the micellar cores in the cluster interior and some exposed to the bulk continuous phase.[48–51] Thus a larger reactor with a higher local monomer concentration available for polymerization in the interface at the 5% BuOH compared with 1%. Additionally, the micelles would act in a cooperative fashion and that monomer molecules in the cluster core had to diffuse through adjacent micellar cores to the exposed reaction interface for chain propagation.

The effect of temperature was perplexing since it demonstrated a nonlinear effect that was significantly less dominant than the effect of BuOH [Fig. 8(A), Table III]. At the lowest temperature, 60°C, the micelles would have the lowest kinetic energy and therefore might cluster together or at least be found in closer proximity to each other. At 70°C, an optimal level of kinetic energy is reached and micelles exist in a comparatively unassociated state. However, at 80°C, a maximum response for M_n was again observed.

Two explanations could elucidate the phenomenon. The kinetic energy of the micelles might be high enough to lead to a significant number of collisions between reactors thereby clustering the cores together. In addition, it has been demonstrated for nonionic amphiphiles with polar moieties that temperature affected their lipophilicity.[18,52,53] The polar groups of these amphiphiles engaged water molecules through hydrogen bonding that are abolished at high temperatures, dehydrating the amphiphiles to render them more lipophilic. Ultimately, self-association of this relatively lipophilic phase prevailed to a larger extent. Since BuOH also engaged water molecules it would also behave as a true amphiphile at high temperatures due to dehydration. Subsequently, self-association of BuOH would be induced, resulting in the increase in M_n.

The nonlinear response of SDS was apparent from the Pareto analysis with the SDS (Q) coefficient assuming a value of −2.419 (Table III). Globally, a parabolic continuance was observed and a minimum was demonstrated at the 4% surfactant concentration [Fig. 8(B)]. The averages of the three groups of minima at 4% SDS were calculated to be 184.7, 247.1, and 271.4 kg mol^{-1}.

The minimum for M_n indicated that 4% surfactant produced the largest quantity of observed particles. Furthermore, it implied that the highest number of micellar reactors that were unassociated formed at

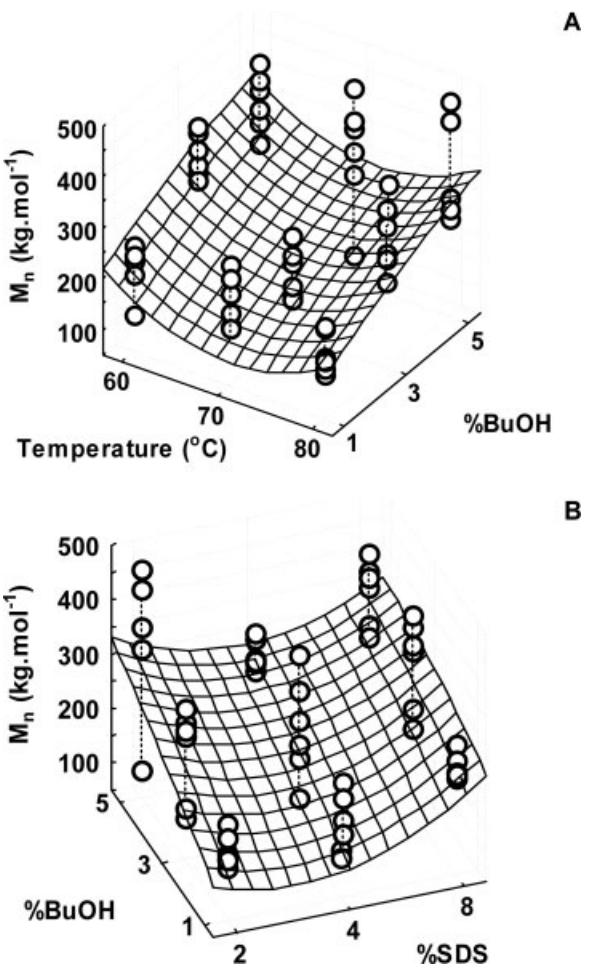

Figure 8 Surface plot of the effects of (A) temperature and cosurfactant (B) surfactant on M_n for P(St-*co*-MMA). While interpreting the surface plots it should be borne in mind that since no significant interactions were noted in the Pareto analysis, the surface plots should be seen to illustrate the effect of a single factor in isolation from the other plotted variable.

4%. At 2% the quantity of surfactant might not be sufficient to produce micelles that would be as small as would be seen at 4%. Since the emulsions were all slightly blue during the reaction process, it could still be assumed that microemulsions were stable, however that the micelles might be slightly larger at 2% (series average M_n of 259.1 kg mol^{-1}) compared with 4% (M_n of 234.6 kg mol^{-1}). At 8% (M_n of 305.5 kg mol^{-1}) micelles might again cluster together since the surfactant tails could associate to some extent and produce micellar aggregates.

The difference between maxima and minima [Fig. 8(B)] were marginal, resulting in a low Pareto coefficient value. At 8% SDS, the cooperative nature of the micellar cores could be suggested to result in a cluster reactor rather than in unassociated micellar reactors as seen at 4% SDS. Even if the individual micelles are of similar size as that at 4%, their true size might be obscured by the clustering effect.

M_w is a true measurement of the amount of monomer assembly in a polymer chain. As shown in Table III, the concentration of BuOH significantly influenced the measured responses in a positively, linear fashion (Pareto coefficient L, +5.086). SDS (Q, −2.257) and temperature (Q, −2.236) also showed significant effects although inferior to that of BuOH.

The linear effect of cosurfactant on polymer weight is again observed from the perspective of the BuOH axis and the nonlinear surfactant effect perpendicular to the SDS axis [Fig. 9(A)]. The continuances of M_w reflected that of M_n suggested a link between the number of reactors found in the microemulsion and the number of units assembled in a chain as evidenced from M_w.

Considering the molecular weight of St and MMA (~ 100 g mol^{-1}) and that the various polymers contained between 2000 and 7500 monomer units based on M_w, it can be suggested that a link existed between the local concentration of the monomers and the polymer weight, again indicating the suggested micellar coagulation phenomenon. If the micelles were associated to a lesser extent at 1% BuOH it would explain why a lower number of monomers were polymerized (series average M_w of 375.9 kg mol^{-1}). Subsequently more pronounced agglomeration was seen as the BuOH increased to 3% (series average M_w of 472.3 kg mol^{-1}) and finally achieved a maximum at 5% (series average M_w of 563.4 kg mol^{-1}), demonstrating a series regression coefficient of $r^2 = 0.9997$.

Judged by the Pareto analyses (Table III), SDS also had a significant effect on monomer assembly as seen from the values of M_w [Fig. 9(A)]. The trends observed for SDS could also be explained by the clustering argument at different surfactant concentrations with M_w values complimentary to that of M_n. The higher values of M_w (compared with their corresponding M_n) illustrated that monomer assembly was not equal in all the reactors. The minimum at 2% SDS (series average M_w of 441.0 kg mol^{-1}) corresponded to the minimum found for M_n. The minimum M_w was also found at 4% SDS and attained a series average value of 422.5 kg mol^{-1} and finally the maximum M_w was found at 8% SDS with a series average 548.1 kg mol^{-1}.

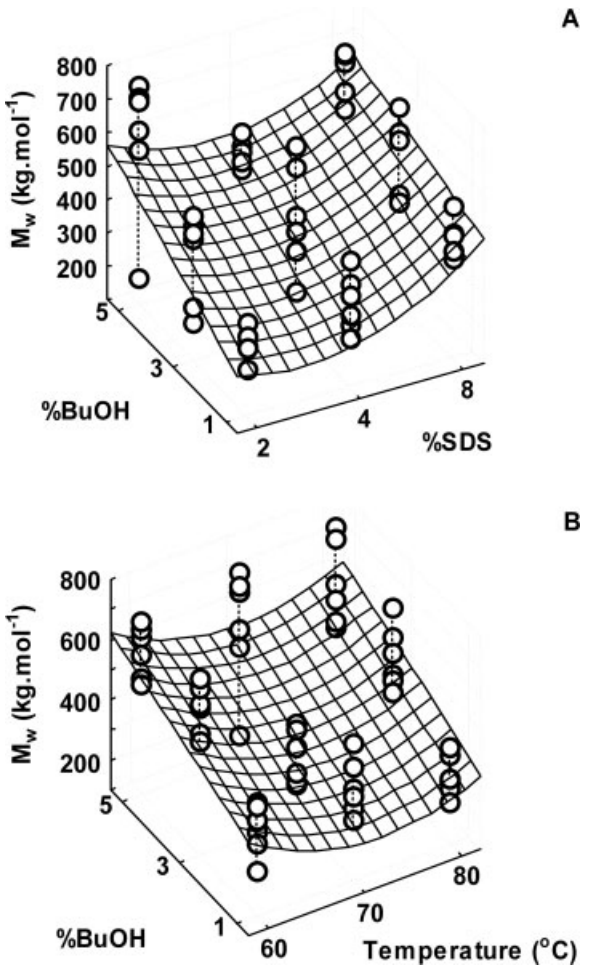

Figure 9 Surface plot of the effects of (A) cosurfactant and surfactant (B) temperature on M_w for P(St-*co*-MMA).

Temperature illustrated its effect on M_w (as with M_n) on particle aggregation with aggregation more prevalent at 60°C and collisions more prevalent at 80°C. Consequently, two series of maxima were observed and depending on the desired weight the temperature could be adjusted to render particles between 200 and 750 kg mol^{-1} [Fig. 9(B)]. The minima was again observed at 70°C and correlated to the fact that the highest number of unassociated reactors were found at this temperature. Note that the effect of BuOH predominated the outcome of final particle properties (Table III).

It was observed that the values of M_w were ~ 100–200 kg mol^{-1} higher than their corresponding

M_n values, resulting in differences in polydispersity, M_w/M_n. The probability of factors having significant effects on the polydispersity was again illustrated with Pareto probability density (Table III).

The polydispersity was fairly broad, exhibiting a range of 1.5–2.1. This reflected the nature of the reaction in the aspect of reactor heterogeneity. Clearly, a vast number of radical species were formed in the micellar environment, each of which resulted in different polymer weight characteristics. However, these values are typical for studies of this type of addition polymerization.[22–24] The linear effect of BuOH was again apparent; however, demonstrated a negative sign to the coefficient (L, −2.892) suggesting that polydispersity was decreased slightly upon an increase in BuOH concentration. The effects of temperature (Q, +2.182) and SDS (+2.326) were also observed to be significant and these showed positive effects (therefore increasing polydispersity) as noted from the signs preceding the magnitude coefficients (Table III). Although the three factors proved significant, they all approached the minimum Pareto significance coefficient of 2.023.

On the basis of these findings it would seem advantageous to incorporate a high concentration of cosurfactant to improve the polydispersity to a minimum. This could arise from the fact that fewer reactors were formed in the microemulsion at 5% cosurfactant compared with the 1% (therefore a relatively high M_n at 5% compared with 1%). The decrease in reactor number could therefore decrease the probability of encountering a high degree of reactor uniqueness. In contrast, the higher the number of reactors, the higher the probability of finding unique micellar reactors that would produce higher polydispersity. Since the number-average weight was lower at 1% BuOH than 5% (Fig. 8) it indicated an increase in the probability of finding a higher reactor count with a resulting higher probability of uniqueness at 1% BuOH.

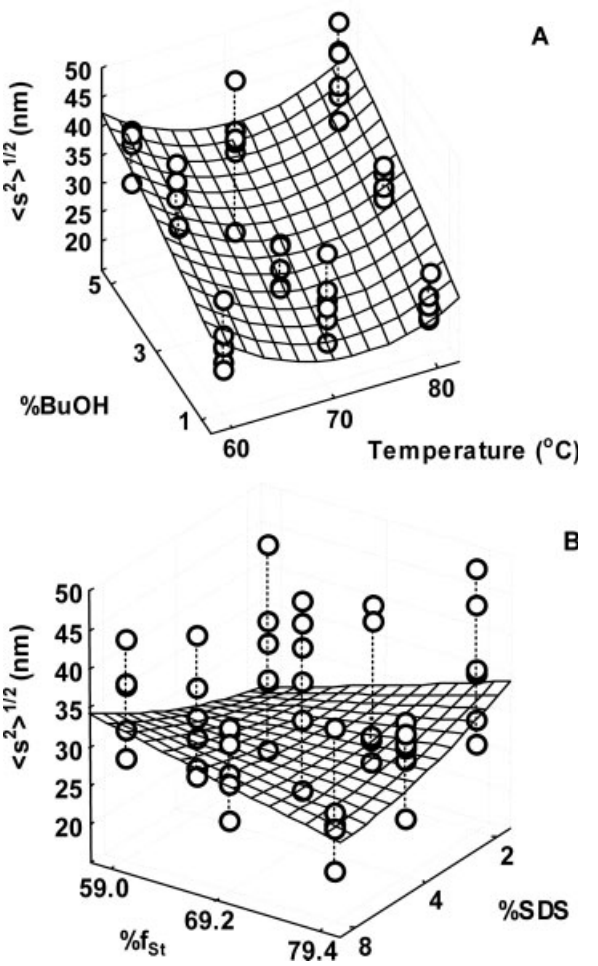

Figure 10 Effect of (A) cosurfactant and temperature (B) surfactant and monomer feed ratio on radius of gyration of P(St-*co*-MMA).

Radius of gyration of P(St-*co*-MMA)

One measure of polymer particle size is the radius of gyration, $\langle s^2 \rangle^{1/2}$.[54,55] As stated earlier the alcohol pseudophase employed as cosurfactant here, could self-associate and since it is located preferentially in the interface, would also associate the micelles into closer proximity to form clusters. From this perspective, the local concentration of monomer at the interface would be relatively higher at 5% BuOH compared with 1%. Consequently, the probability of particle propagation would be higher with longer chains forming during the polymerization. The clustering effect could also decrease the surface area available for termination reactions (in competition with propagation reactions). Therefore, an increase in BuOH concentration resulted in a linear increase in $\langle s^2 \rangle^{1/2}$ from $\sim$ 20 to 45 nm (L, +5.249, r^2 = 0.9958).

Clearly, all the reactions resulted in the production of nanoparticles according to the definition of nanoparticles, i.e., particles with at least one length dimension between 0.1 and 100 nm.[56] The average $\langle s^2 \rangle^{1/2}$ of the 1% BuOH category was $\sim$ 26 nm, the 3% category averaged $\sim$ 32 nm, and the 5% BuOH produced an average of 37 nm [Fig. 10(A)].

The effect of temperature on the particle size was less dominant; however, still significant compared to the effect of the cosurfactant. As seen for changes in M_n, temperature exerted a quadratic effect (Q, −3.005), implicating more complex mechanisms of action involved in its effects as stated earlier. At the lowest temperature, the micelles would have the lowest kinetic energy and therefore might cluster together or at least be found in closer proximity (series average [$\langle s^2 \rangle^{1/2}$ of $\sim$ 35 nm). At 70°C, an optimal level of kinetic energy is reached and micelles exist

in a comparatively unassociated state and therefore resulted in the lowest average for $\langle s^2 \rangle^{1/2}$ of $\sim$ 28 nm. Since radical termination could also prevail at this temperature, particle growth could be curbed to a maximum at 70°C. At 80°C a second maximum response for $\langle s^2 \rangle^{1/2}$ was again observed with a series average of $\sim$ 32 nm, due to an increase in reactor collision.

There was a significant linear by linear interaction between SDS concentration and monomer ratio (L by L, −2.446) since a simultaneous linear by linear increase or decrease in both SDS concentration and feed ratio resulted in a decrease in radius of gyration [Table III, Fig. 10(B)]. If seen from a concentration of 2% surfactant, the increase in mole fraction ratio (e.g., an increase in St mole fraction) resulted in an increase in the particle size. If seen from 4% surfactant, virtually no change in the response was seen with an increase in feed ratio. Therefore, the results for 8% SDS clearly contradicted the observations at 2%, having illustrated a relative decrease in radius of gyration as a function of an increase in mole fraction ratio (f_{St}). Figure 11 shows the distribution of particle sizes as classified by cosurfactant concentration. Reasonable separation of distinct particle size and distribution could be obtained by changing the cosurfactant concentration from 1 to 5% with 3% producing some overlap between both categories.

One explanation for the interaction phenomenon could be that an increase f_{St} resulted in an increase in the styrene content of the copolymers. Conversely, the MMA content decreased and its amphiphilic effect might be less prominent when compared with higher MMA interfacial abundance. It would seem that the higher contribution of MMA to surface tension reduction would result in smaller particles, since micelles could be stabilized at a relatively low concentration of SDS. It would support, from this perspective, that surfactant aggregation would probably be minimized, preventing micellar agglomeration. The function of interfacial MMA as cosurfactant (although significantly eclipsed by the cosurfactant function of BuOH) is therefore plausible.

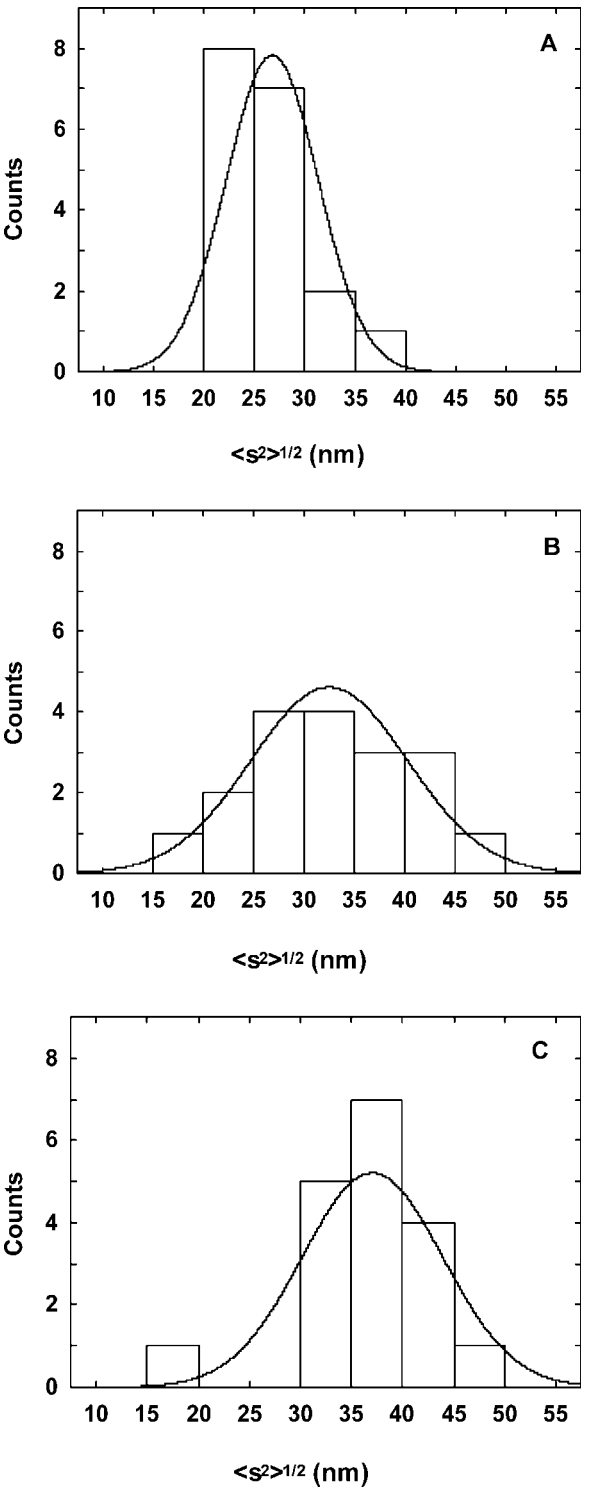

Figure 11 Radii of gyration of all samples categorized according to BuOH (A) 1% (average of 26 nm), (B) 3% (average of 32 nm), and (C) 5% (average of 37 nm).

Conformational analysis

Conformational analysis was also performed to study the bulk chain conformation of the copolymers. The conformation of polymer chains is the result of intra and intermolecular force interactions between polymer–polymer and solvent-polymer associations. Solubility in the solvent could have a significant influence on polymer conformation with different solvent inducing compact through extended conformations of the polymers.[57,58] The copolymer weights (Table II) varied between 200 and 750 kg mol^{-1} for P(St-*co*-MMA) measured in THF. Since these polymers all approached the maximum solubility in THF, they could not show significant extension.

The data in Table II show that q was very close to 0.5 indicating that the majority of the polymers (data

not shown) demonstrated a random coil conformation at or just below the theta condition. This means that the solvent has separated a cluster of chains; however, limited expansion of the chains occurred and a more compact conformation was still present. Pareto analysis of copolymer conformation did not reveal statistically significant effects (Table III); however, could still rank the factors and magnitude of the effects. Again, it was clear that the cosurfactant prevailed to be the most dominant factor. These observations could probably be related to the effect that the interfacial cosurfactant had the most profound impact on the polymer size and weight properties during the synthesis. Consequently, the effect on conformation should also be related to the effect of cosurfactant.

CONCLUSIONS

The dominating effect of the cosurfactant, BuOH, clearly prevailed in the microemulsion copolymerization of styrene and MMA. The linear increases observed for molecular weight and particle size with an increasing concentration of BuOH could be exploited for the successful production of a series of nanoparticles, while the composition was virtually unaffected by the cosurfactant. It is suggested that the preferential location of the cosurfactant at the oil/water interface resulted in a clustering effect that affected the reactor number and size and subsequently the molecular weight and radius of gyration of the nanoparticles. Factors including temperature and surfactant modulated the clustering effect; however, were shown to be inferior based on Pareto analysis. Additionally, as observed from compositional analysis, the feed ratio of the monomers dominated the polymer composition and served as an approximate template for the polymer composition.

References

1. Stoffer, J. O.; Bone, T. J Dispersion Sci Technol 1980, 1, 393.
2. Stoffer, J. O.; Bone, T. J Polym Sci Part A: Polym Chem 1980, 18, 2641.
3. Puig, J. E.; Corona-Galvan, S.; Maldonado, A.; Schulz, P. C.; Rodriguez, B. E.; Kaler, E. W. J Colloid Interface Sci 1990, 137, 308.
4. Candau, F. Macromol Symp 1995, 92, 169.
5. Puig, J. E.; Mendizabal, E.; Rodriguez, B. E.; Rabelero, V.; Velazquez, R.; Castano, V. Int J Polym Mater 1995, 30, 167.
6. Capek, I.; Juranicova, V. J Polym Sci Part A: Polym Chem 1996, 34, 575.
7. Danielsson, I.; Lindman, B. Colloids Surf 1981, 3, 391.
8. Blokhus, A. M.; Høiland, H.; Gjerde, M. I.; Ersland, E. K. J Colloid Interface Sci 1996, 179, 625.
9. Førland, G. M.; Rahman, T.; Høiland, H.; Børve, K. J. J Colloid Interface Sci 1996, 182, 348.
10. Maidment, L. J.; Chen, V.; Warr, G. G. Colloids Surf A 1997, 331, 129.
11. John, A. C.; Rakshit, A. K. Colloids Surf A 1995, 95, 201.
12. Khadir, A.; Roux-Desgranges, G.; Roux, A. H. Thermochim Acta 1997, 292, 59.
13. Abuin, E.; Lissi, E.; Olivares, K. J Colloid Interface Sci 2004, 276, 208.
14. Pokhriyal, N. K.; Devi, S. Eur Polym Mater 2000, 36, 333.
15. Alany, R. G.; Rades, T.; Agatonovic-Kustrin, S.; Davies, N. M.; Tucker, I. G. Int J Pharm 2000, 196, 141.
16. Sarma, S.; Bora, M.; Dutta, R. K. Colloids Surf A 2005, 256, 105.
17. Ganesh, T.; Balamurugan, D.; Sabesan, R.; Krishnan, S. J Mol Lip 2006, 123, 80.
18. Lobo, L.; Svereika, A. J Colloid Interface Sci 2003, 261, 498.
19. Rubio, D. A. R.; Zanette, D.; Nome, F.; Bunton, C. A. Langmuir 1994, 10, 1151.
20. Tomšic, M.; Bešter-Rogač, M.; Jamnik, A.; Kunz, W.; Touraud, D.; Bergmann, A.; Glatter, O. J Colloid Interface Sci 2006, 294, 194.
21. Attwood, D.; Terreros, A.; Lopez-Cabarcos, E.; Galera-Gomez, P. A. J Colloid Interface Sci 2000, 225, 25.
22. Gómez-Cisneros, M.; Treviño, M. E.; Peralta, R. D.; Rabelero, M.; Mendizábal, E.; Puig, J. E.; Cesteros, C.; López, R. G. Polymer 2005, 46, 2900.
23. Shi, Y.; Wu, Y.; Hao, J.; Li, G. Colloids Surf A 2005, 262, 191.
24. Puig, J. E.; Mendizábal, E.; Delgado, S.; Arellano, J.; López-Serrano, F. C R Chim 2003, 6, 1267.
25. Tauer, K.; Ramírez, A. G.; López, R. G. C R Chim 2003, 6, 1245.
26. Hofe, T.; Koenigsmann, H. GIT Labor-Fachzeitschrift 2003, 47, 380.
27. Kendrick, B. S.; Kerwin, B. A.; Chang, B. S.; Philo, J. S. Anal Biochem 2001, 299, 136.
28. Mhatre, R.; Krull, I. S. Anal Chem 1993, 65, 283.
29. Zimm, B. H. J Chem Phys 1948, 16, 1093.
30. Zimm, B. H.; Stockmayer, W. H. J Chem Phys 1949, 17, 1301.
31. Wyatt, P. J. Anal Chim Acta 1993, 272, 1.
32. Liu, Y.; Bo, S.; Zhu, Y.; Zhang, W. Polymer 2003, 44, 7209.
33. De Gennes, P. G. Scaling Concepts in Polymer Physics, Cornell University Press: Ithaca, NY, 1979.
34. Jovin, T. M.; Morris, S. J.; Striker, G.; Schultens, H. A.; Digweed, M.; Arndt-Jovin, D. J. J Histochem Cytochem 1976, 24, 269.
35. Clasen, C.; Kulicke, W.–M. Prog Polym Sci 2001, 26, 1839.
36. Masson, J.-F.; Pelletier, L.; Collins, P. J Appl Polym Sci 2001, 79, 1034.
37. Prasad, A. Polym Eng Sci 1998, 38, 1716.
38. Qin, D. Appl Spectrosc 2001, 55, 871.
39. Karami, A.; Balke, S. T.; Schunk, T. C. J Chromatogr A 2001, 911, 27.
40. Juran, J. M. In Juran's Quality Handbook, 5th ed.; Juran, J. M.; Godfrey, A. B.; Hoogstoel, R. E.; Schilling, E. G., Eds.; McGraw-Hill: New York, 1999; Chapter 5.
41. Pareto, V. J Political Economy 1897, 5, 485.
42. Deb, K.; Mitra, K.; Dewri, R.; Majumdar, S. Chem Eng Sci 2004, 59, 4261.
43. Massebeuf, S.; Fonteix, C.; Hoppe, S.; Pla, F. J Appl Polym Sci 2003, 87, 2383.
44. Moshinsky, L.; Figovsky, O. L. Sci Israel Technol Adv 1999, 1, 28.
45. Carraher, C. E. Polymer Chemistry, 5th ed.; Marcell Dekker: New York, 2000.
46. Möller, A.; Lang, P.; Findenegg, G. H.; Keiderling, U. J Phys Chem B 1998, 102, 8958.
47. Marinov, R.; Panayotova, S.; Dehrzhanski, A. Prog Colloid Polym Sci 2001, 118, 256.

48. Lianos, P.; Lang, J.; Zana, R. J Phys Chem 1982, 86, 4809.
49. Lianos, P.; Lang, J.; Strazielle, C.; Zana, R. J Phys Chem 1982, 86, 1019.
50. Sjoeblom, E.; Henriksson, U.; Stenius, P. Finnish Chem Lett 1982, 114, 6.
51. Roux-Desgranges, G.; Roux, A. H.; Grolier, J. P. E.; Viallard, A. J Solution Chem 1982, 11, 357.
52. Von Rybinski, W.; Guckenbiehl, B.; Tesmann, H. Colloids Surf A 1998, 142, 333.
53. Aramaki, K.; Ozawa, K.; Kunieda, H. J Colloid Interface Sci 1997, 196, 74.
54. Kosmas, M. K. J Phys A: Math Gen 1981, 14, 2779.
55. Suzuki, K. Bull Chem Soc Jpn 1947, 20, 19.
56. National Nanotechnology Institute. What is nanotechnology? Available at http://www.nano.gov/html/facts/whatIsNano.html.
57. Gan, H. H.; Eu, B. C. J Chem Phys 2011 1998, 109.
58. Flory, P. J. Statistical Mechanics of Chain Molecules; Hanser Gardner: New York, 1988.